INTUITIVE MACHINES (IM-1) LUNAR LANDING SITE: THE VIEW FROM ORBIT. B. J. Thomson[1] and C. A. Nypaver[2], G. W. Patterson[3], A. M. Stickle[3], and J. T. S. Cahill[3], [1]Dept. of Earth, Environmental, and Planetary Sciences, University of Tennessee, Knoxville, TN (bthom@utk.edu), [2]National Air and Space Museum, Smithsonian Institution, Washington, DC, [3]Johns Hopkins University Applied Physics Laboratory, Laurel, MD.

Introduction: A major milestone for the commercial lunar sector was attained by Intuitive Machines lander *Odysseus* (IM-1), which successfully soft-landed near the lunar south pole on February 22, 2024. Despite coming to rest at an unplanned angle of ~30°, the spacecraft was able to communicate with Earth and remained operational for a week on the lunar surface.

Here we use available orbital data to characterize the geologic context of the IM-1 landing site, with an emphasis on Mini-RF bistatic radar data, LROC image data, and LOLA and LROC topographic data [1-3]. Part of the science goals of the Lunar Reconnaissance Orbiter (LRO)'s extended mission is to support future lunar landings by analyzing orbital data over future, current, and past landed missions in order to better constrain and "ground truth" the orbital data. A number of surface images were also returned by the ILO-X (International Lunar Observatory) cameras onboard the lander [4], but the off-nominal deployment geometry makes it difficult to directly compare with orbital data.

IM-1 Mission overview: The IM-1 *Odysseus* mission was the second launch of the NASA's lunar CLPS (Commercial Lunar Payload Services) program and the first to successfully reach the Moon. Payload elements include contributions that were competitively selected by NASA as well as paid for by private sector partners. The lander (also known as Nova-C) is a hexagonal cylinder in shape and descended to the surface on a single gimbled main engine aided by thrusters [5].

Landing site location: *Odysseus* touched down in an intercrater region about 10° from the lunar south pole (~300 km) at 80.13°S 1.44°E. The landing site (**Fig. 1a**) lies east of the irregular degraded crater Malapert A (33 km in diameter) and roughly equidistant between craters Malapert B, Malapert C, and Malapert K (32, 38, and 39 km in diameter, respectively). Notably, the site is very close to the ring of discontinuous massifs that constitute the outer rim of South Pole-Aitken Basin [e.g., 6].

Prior geologic mapping: The lunar south polar region was initially mapped using Lunar Orbital images at a scale of 1:5M in 1979 [7]; this linework was digitized and remapped in 2013–2020 by [8, 9] using LROC WAC mosaics [3] and LOLA topography [2]. The *Odysseus* landing site lies in geologic unit pNt: pre-Nectarian terra material. This geologic unit is described as forming moderately rugged to rugged, diverse terrain, including degraded partial crater rims and lower intervening tracts. It is interpreted to be degraded equivalents of Imbrian and Nectarian basin, terra, and plains materials [7, 8].

More recent re-mapping of the south polar region at a scale of 1:300k was conducted [10] that mapped this region as being unit Isc2, an annular region of Upper Imbrian-aged crater materials that surrounds Schomberger crater. These inferred younger deposits may be a relatively thin veneer over the pre-Nectarian massifs, but their thickness remains to be determined.

Mini-RF bistatic data: The Mini-RF instrument has been operating in a bistatic configuration since 2011 following a transmitter failure. In this operational mode, a ground-based radiotelescope transmits a polarized radio signal at a targeted region on the lunar nearside, and the Mini-RF antennae receives the energy bounced off the lunar surface. The instrument can receive both S-band (12.6 cm wavelength, 2.38 GHz) and X/C band radar wavelengths (4.2 cm wavelength, 7.14 GHz). Below we focus on an X-band bistatic observation over the *Odysseus* site; analysis with δ-CPR data [11] is ongoing.

Results: The landing site was as expected in that it is a typical highlands site that consists of mostly low, rolling terrain interrupted by craters; steep slopes are largely limited to crater interior walls (**Fig. 1**). Prior analysis of lunar slopes indicates that there is a greater proportion of steep slopes moving toward the equator [12], a finding consistent with a predicted latitudinal difference in the lunar cratering rate [13]. Yet even though there are fewer steep slopes at high latitudes, almost 30% of the terrain covered by the Mini-RF swath given in **Fig. 1b** exceeds a slope of 10°, constituting a landing hazard. No high concentrations of rough-textured ejecta or hazardous boulders that are commonly found surrounding fresh craters were observed in the radar data, a finding consistent with the near-surface view (**Fig. 1d**). Unlike on the mare, small craters in the highlands (<5 to 10 km in diameter) tend not to excavate many boulders [e.g., 14]. Therefore, the lack of a radar signature consistent with abundant rocks is consistent with Diviner-derived rock abundance measurements for non-polar terra regions are generally low (rocks occupy <0.5% of the surface [15]), but these data do not extend to high latitudes due to the challenges posed by low temperatures and the significant influence of slopes on surface temperatures at higher latitudes that persists throughout the lunar night.

Discussion: Landing site characterization is a key element in planetary surface exploration as a mission that does not land safely is over before it begins. Even degraded craters still possess slopes that may constitute a hazard, emphasizing the need and utility of terrain relative navigation. Mini-RF radar data can help probe for rock hazards and aid in unraveling the chronology of overlapping crater deposits. But the radically different appearance of the lunar surface at different spatial scales means that nested geologic maps over a variety of spatial scales are likely necessary to better constrain sample provenance for future missions.

Acknowledgments: We thank the IM-1 and LRO teams for their tireless efforts to make these missions a success and to distribute these data to the public.

References: [1] Patterson G. W. et al. (2017) *Icarus*, *283*, 2–19. [2] Neumann G. A. (2011, doi:10.17189/1520642. [3] Robinson M. S. et al. (2010) *Space Sci. Rev.*, *150*, 81–124. [4] Durst S. (2022) *AAS Meeting #240*, 431.404. [5] Bussey D. B. J. and Martin T. (2024) *LPS LV*, abstract #1931. [6] Garrick-Bethell I. and Zuber M. T. (2009) *Icarus*, *204*, 399–408. [7] Wilhelms D. E. et al. (1979) *USGS Map I-1162*, 1:5M scale. [8] Fortezzo C. M. et al. (2020) *LPSC VI*, abstract #2760. [9] Fortezzo C. M. and Hare T. M. (2013) *LPSC XLIV*, abstract #2114. [10] Krasilnikov S. et al. (2023) *Icarus*, *394*, 115422. [11] Fassett C. I. et al. (2024) *PSJ*, *5*, 4. [12] Kreslavsky M. A. and Head J. W. (2016) *Icarus*, *273*, 329–336. [13] Le Feuvre M. and Wieczorek M. A. (2011) *Icarus*, *214*, 1–20. [14] Bart G. D. and Melosh H. J. (2010) *JGR*, *115*, E08004. [15] Bandfield J. L. et al. (2011) *JGR*, *116*, E00H02.

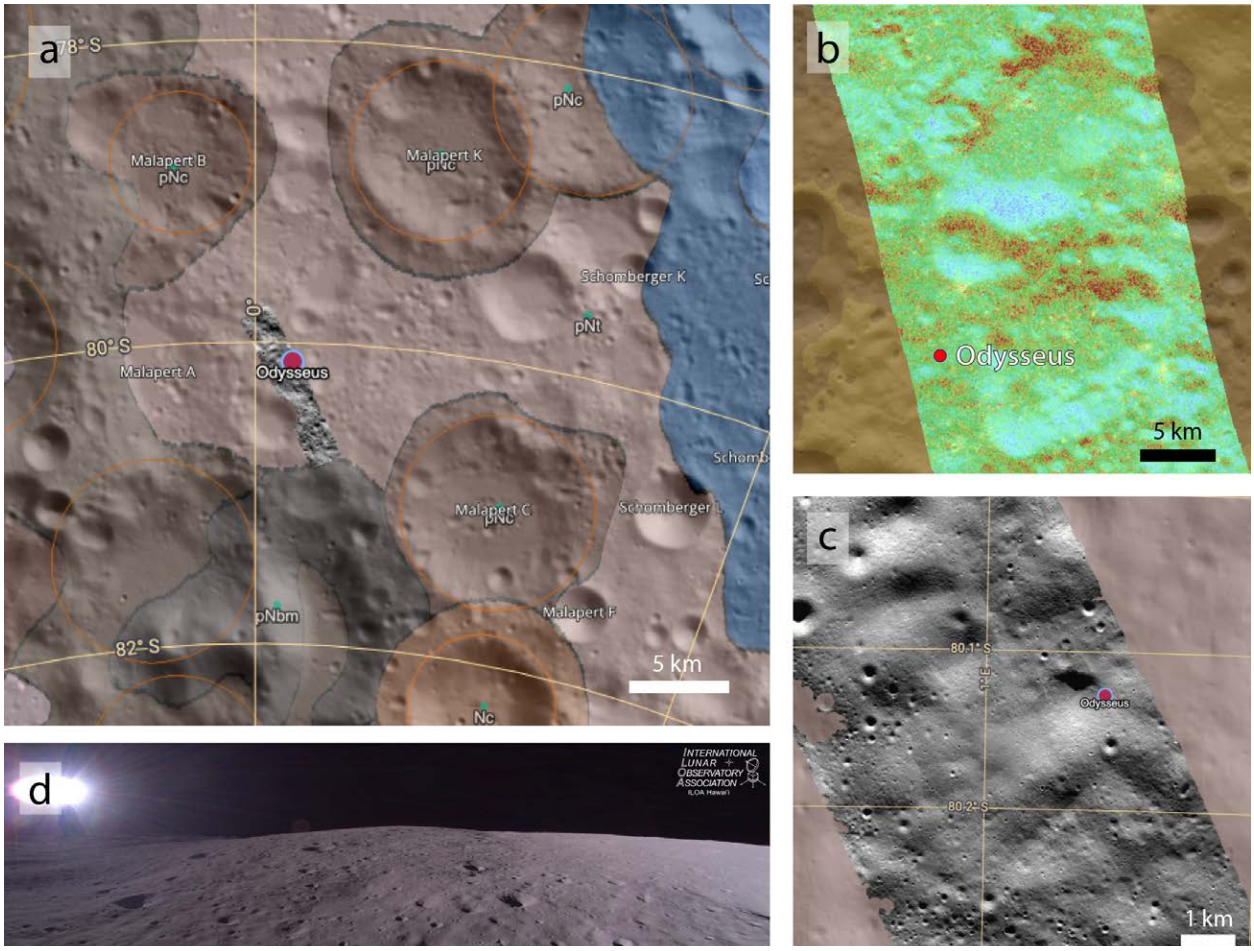

Figure 1. (a) LDEM2015 shaded relief map of IM-1 landing site overlain with a 1:5 M geologic map [7, 8]. Odysseus lander is marked with red circle. **(b)** Mini-RF X-band bistatic swath (LXT_67327_1S1_XIU_84S012_V1), total power image with colorized CPR overlain (100 m/pixel spatial resolution; red = higher CPR values). **(c)** LROC NAC orthomosaic made from NAC images M1435274280 L/R (0.85 m/pixel; data credit NASA/Goddard/ASU). **(d)** Panoramic Image acquired 13 seconds before landing by the ILO-X instrument [4].